INFLUENCE OF THE ANGLE OF ATTACH ON THE LEADING EDGE BUBBLE IN A FLOW OVER A THIN FLAT PLATE

André Luiz Tenório Rezende, arezende@ime.eb.br
Fernando Araújo, fernandonaraujo@click21.com.br
Department of Mechanical and Materials Engineering, IME - Military Engineering Institute, 22290-270, Rio de Janeiro, RJ, Brazil

Angela Ourivio Nieckele, nieckele@puc-rio.br
Department of Mechanical Engineering, PUC/Rio, 22453-900, Rio de Janeiro, RJ, Brazil

Abstract *The objective of this investigation is the numerical simulation of the flow over an inclinated thin flat plate. In this complex flow the existence of laminar-to-turbulent transition, boundary layer separation, leading edge bubble and reattachment turns the numerical prediction a considerable challenge. Leading edge bubbles found in flat plate flow will usually exist in stabilization fin of missiles and rockets, and these bubbles have significant influence on the pressure distribution and lift generated by such fins. The shape and structure of the separation region itself has significant impact on the pressure peak near the leading edge which is the primary contributor to the lift on a fin. The influence of the leading edge bubble extends well downstream of the reattachment point and the interaction between the leading edge bubble and the trailing edge separation region is poorly understood. The purpose of the present work is to analyze the influence of the angle of attack on the leading edge bubble and the reattachment point. This is a part of a simulations series of the incompressible flow around a thin flat plate with a leading edge and an infinite wingspan at small incidences. Simulations were accomplished for inclination angles of the flat plate varying from 1 to 5 degrees with a Reynolds number of 2.13 × 10e5. The solutions are obtained through the Reynolds Averaged Navier-Stokes (RANS) equations for the two-dimensional steady state flow, using the Spalart-Allmaras and SST κ-ω models. These RANS models assume isotropic modeling of the Reynolds tensor. The results are compared with available wind tunnel experimental data.*

Keywords*: flat plate, shallow incidence, RANS, reattachment*.

1. INTRODUCTION

This paper is a numerical investigation of the incompressible turbulent flow around a thin flat plate with a sharp leading edge and an infinite wingspan from 1 to 5 degrees (Fig. 1a). The flow around a thin plate at small incidence angles presents a very complex structure, presenting laminar-to-turbulent transition, boundary layer separation, leading edge bubble, reattachment, relaminarization and a secondary recirculation bubble.

The study of the flow around the thin flat plate at shallow incidence can help in the design of fins and wings for projectiles and missiles. The flow around an inclined flat plate with a sharp leading edge, as shown in Fig. 1a, induces a long and thin bubble, denominated "thin aerofoil bubble" (Gault, 1957). The boundary layer around the leading edge is very thin, and it is expected to separate immediately, due to the flow direction change. As shown in Fig. 1a, there is a dividing streamline which separates the main bubble from the outer flow and which rejoins the surface at the reattachment point. If the incidence angle is sufficiently small (usually smaller than 6 degrees), the flow reattaches at the upper surface at a point which moves gradually downstream with increasing incidence angle. For greater angles, there is no reattachment point, and the bubble enlarges downstream into the wake (Newman and Tse, 1992). Due to the fixed separation point the flow is insensitive to a change in Reynolds number, and transition will occur soon after separation (Crompton, 2000).

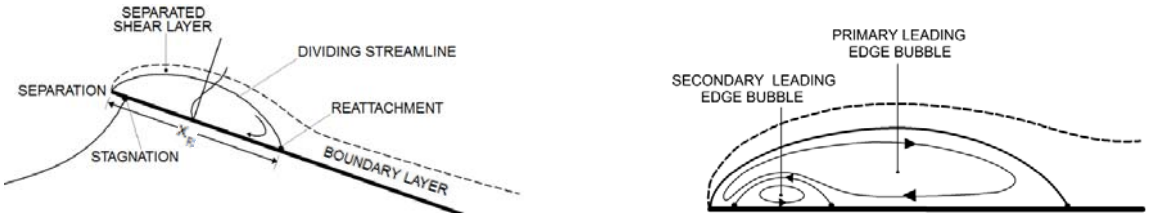

(a) Simplified model **(b) Sketch of the secondary bubble**

Figure 1. Simplified model of long and thin bubble.

After the separation, the shear layer suffers transition very close to the leading edge. The turbulent shear layer increases quickly and has a high entrainment rate; it then reattaches (reattachment point X_R) further downstream and bifurcates. Part of the flow is directed to upstream to feed the shear layer. The resultant backflow reduces the pressure at

the surface and helps to bend the shear layer back to the reattachment point. The remaining flow is driven downstream where reverts gradually to an attached turbulent boundary layer before reaching the trailing edge (assuming there is enough length left after reattachment).

The fluid flowing upstream the plate is subject to a strong favorable pressure gradient and subsequently it accelerates and reaches a maximum reversed velocity at approximately half way back along the length of the bubble. This favorable pressure gradient has a stabilizing effect on the reverse flow boundary layer and a significant drop in turbulence intensity is recorded over this region. Corresponding to this drop in turbulence intensity, the velocity gradient near the surface reduces and the boundary layer profiles become more laminar-like; the favorable pressure gradient induces a relaminarisation (reverse transition).

Near the front of the separation bubble the pressure gradient is adverse to the reverse flow and consequently the laminar-like boundary layer is prone to separate. Crompton (2000) observed a small secondary separation bubble in his experiments near the leading edge of the plate. This second very small bubble is schematically illustrated in Fig. 1b and it is very hard to be predicted by RANS models. The length of this separation bubble varies with both incidence angle and local Reynolds number. The local Reynolds number dependence is caused by the relaminarisation process in the reversed flow boundary layer which itself is dependent on the local velocity.

Due to the presence of those several flow structures, this type of problem poses a severe challenge to the ability of the turbulence models to predict the flow. The simulations were accomplished with models based in the Reynolds Average Navier-Stokes equations (RANS), with high Reynolds number.

This complex flow around a plate at the shallow incidence has been experimentally investigated by Crompton (2000). Detailed velocity and turbulence statistics were measured in wind tunnel for the leading edge bubble with the use of Laser Doppler Anemometry (LDV) for inclination angles of the flat plate varying from 1 to 5 degrees with a Reynolds number based on the chord c equal to 2.13×10^5. He showed that the Reynolds number did not influence the flow. The turbulence models performance are evaluated by comparing with Crompton's experimental data (Crompton, 2000).

A few numerical works can be found in the literature, employing the same flow conditions and geometry as Crompton (2000) like Collie et al. (2008), Sampaio et al. (2006), Rezende et al. (2008) and Rezende and Nieckele (2009).

Collie et al. (2008) studied the flow considering incidence angles α equal to 1^0 and 3^0, with the following two equation turbulence RANS models: κ–ω (Wilcox,1998) and SST κ–ω (Menter, 1994), in a two dimensional domain. Collie was not able to obtain results for $\alpha = 5^o$ and affirmed that RANS models would not be capable to capture the secondary recirculation bubble.

Sampaio et al. (2006) proposed the Forced Sub-Grid Model for Large Eddy Simulation (f-LES) to investigate the problem with a three dimensional transient formulation. Due to limited computational resources, Sampaio et al. (2006) simulated only the inclination angle $\theta = 1^0$ in a reduced domain and relatively coarse mesh. Although better results were obtained in relation to the RANS models predictions, it was concluded that a more refined mesh was needed and the RANS models were no capable of capturing the secondary bubble.

Rezende et al. (2008) employed the Reynolds Stress Model - RSM (Launder, 1989) and the v^2f model (Durbin,1995) to capture the turbulence anisotropy, for $\theta = 1^o$. Better predictions were obtained with the RSM model only for the second order statistics, while poor results were predicted with the v^2f model, especially for high Reynolds numbers. This work also concludes that the RSM and v^2f models present difficulties for simulation with other θ angles.

Rezende and Nieckele (2009) simulated the problem through the Large Eddy Simulation - Dynamic Smagorinsk Model (Germano et al., 1991; Lilly, 1992) for $\theta = 1^o$. In this case, it was used a refined mesh near leading edge and parallel processing, obtaining better results for 1 degree incidence angle.

Based on the results and conclusions of the previous papers, this paper investigates numerically new results for the flow for $\theta = 1$ to 5 degrees using two different methodologies: Spalart-Allmaras (Spalart and Allmaras, 1992) and SST κ–ω model. The mesh was significantly refined mesh, in order to guarantee $y^+ \approx 1$ at the first grid point near the plate. The one-equation Spalart-Allmaras model was chosen due to its outstanding performance in aerodynamic problems, while the two-equation SST κ–ω model was selected because it presented the best result with the RANS methodology in previous investigations (Rezende et al, 2008).

2. MATHEMATICAL MODEL

The Reynolds-averaged approach is based on decomposing the velocity as $\mathbf{u} = \overline{\mathbf{u}} + \mathbf{u}'$ where $\mathbf{u}$ is the average velocity vector and $\mathbf{u}'$ the velocity vector fluctuation. The average continuity and momentum equation (RANS), for a steady state incompressible flow is given by

$$\nabla \bullet \overline{\mathbf{u}} = 0 \quad ; \quad \nabla \bullet (\overline{\mathbf{u}}\,\overline{\mathbf{u}}) = -\nabla\left(\frac{p}{\rho}\right) + \upsilon \nabla^2 \overline{\mathbf{u}} + \nabla \bullet \left(-\overline{\mathbf{u}'\,\mathbf{u}'}\right) \tag{1}$$

where ρ is the density, $\upsilon = \mu/\rho$ is the cinematic viscosity, μ is the molecular viscosity, p is the pressure. Equation (1) has the same form of the Navier-Stokes equation, but now it has an additional term, the turbulent Reynolds stress term, $-\overline{\mathbf{u}'\,\mathbf{u}'}$, representing the influence of the fluctuation on the average flow. In order to close Eq. (1), the turbulent Reynolds stress can be modeled based on the Boussinesq hypothesis, where the turbulent stress is obtained through an

analogy with Stokes law, i.e., the stress is proportional to the deformation rate. The turbulence models selected to be investigated at the present work are described next.

2.1. SST *k-ω* MODEL

The Shear-Stress Transport (SST) κ–ω RANS model (Menter, 1994) was proposed for aeronautical flows simulations with strong adverse pressure gradients and separation by combining the κ–ε and κ–ω models. For boundary layers flows, the κ–ω model is superior to the κ–ε model in the solution of the viscous near-wall region, and has been applied with success in problems involving adverse pressure gradients. However, the κ–ω model requires a non-zero boundary condition on ω for non-turbulent free-stream, and the calculated flow is very sensitive to the specified value (Menter, 1994). It has also been shown (Cazalbou *et al* , 1993) that the κ-ε model does not suffer this deficiency. Therefore, the SST κ–ω model blends the robust and precise formulation of the κ–ω model close to walls with the free-stream independence of the κ–ε model outside the boundary layer. To accomplish this, the κ–ε model is written in terms of the specific dissipation rate, ω. Then, the standard κ–ω model and the transformed κ–ε model are both multiplied by a blending function and both models are added together. This blending function F_1 is zero (leading to the standard κ–ω model) at the inner edge of a turbulent boundary layer and set to a unit value (corresponding to the standard κ–ε model) at the outer edge of the layer.

The turbulent eddy viscosity is formulated as follows:

$$\upsilon_t = \frac{\kappa / \omega}{\mathbf{max}\left(1\,;\, S F_2 /(0.31\,\omega)\right)} \quad ; \quad F_2 = \tanh\left(\Phi^2\right) \quad ; \quad \Phi = \max\left(\frac{2\sqrt{\kappa}}{0.09\,\omega\, d}; \frac{500\,\upsilon}{d^2\omega}\right) \tag{2}$$

where $S = (2\ \overline{S_{ij}}\ \overline{S_{ij}})^{0.5}$ is the modulus of the mean rate-of-strain tensor $\overline{S_{ij}}$, and F_2 is the blending function for the turbulent eddy viscosity in the SST κ–ω model, d is the distance to the wall. The turbulent kinetic energy κ and specific dissipation rate ω of the SST κ–ω model (Menter, 1994) can be determined by the solution of its conservation equations, where the set of closure constants for the SST κ–ω model ϕ are calculated using a blend between the constants ϕ_1 of the standard κ–ω and and ϕ_2 of the κ–ε model as $\phi = F_1\ \phi_1 + (1 - F_1)\ \phi_2$.

2.2. SPALART-ALLMARAS MODEL

Developed by Spalart and Allmaras (1992), this is a model relatively simple that solves a transport differential equation for the turbulent viscosity and, therefore, it requests smaller computational effort. The Spalart-Allmaras model was designed specifically for aerospace applications involving wall-bounded flows and adverse pressure gradients. The differential equation is derived by using empiricism, arguments of dimensional analyses and selected dependence on the molecular viscosity. For this model, the turbulent Reynolds stress is modeled without the last term of Eq. (3), as

$$\overline{u_i' u_j'} = -\,2\,\overline{S_{ij}}\,\upsilon_t \tag{3}$$

The eddy viscosity is defined as

$$\upsilon_t = \tilde{\upsilon}\ f_{v1} \qquad ; \qquad f_{v1} = \frac{\chi^3}{\chi^3 + C_{v1}^3} \qquad ; \quad \chi \equiv \frac{\tilde{\upsilon}}{\upsilon} \tag{4}$$

where $f_{\upsilon 1}$ is a viscous damping function used to treat more appropriate the buffer layer and viscous sublayer. The transport equation for the working variable $\tilde{\upsilon}$ is given by (Deck et al, 2002) and C_{v1} = 7.1 .

3. RESULTS

The thin flat plate proposed by Crompton (2000) was modeled with the geometry described in Fig. 2. The plate has a chord length c of 160 mm and a span of 800 mm giving an aspect ratio of 5, which is sufficient to supply nominally two-dimensional flow.

The reattachment length was found by Crompton (2000) to be independent of Re above 10^5, where Re is defined as $Re = U_\infty c / \upsilon$, where U_∞ is the free stream velocity, and c the chord length. The wind tunnel investigation was carried at $Re = 2.13 \times 10^5$ and this Reynolds number is used to compare the turbulence models and the experiments. Attack angles, θ = 1 to 5 degrees, are available in experimental data in 1 degree intervals. At inclination of 5 degrees the flow is separated for the majority of the length of the plate. The LDV measurements for the mean velocity and a few

turbulent quantities over the plate are available at Crompton´s study (2000).

Figure 3 shows the computational domain used in simulations, which was defined based on the work of Collie (2008). At the inlet, the cartesian components of velocity are set according to the angle of attack and the turbulence intensity of the freestream defined as $\varsigma = (1/3)(\overline{u'u'} + \overline{v'v'} + \overline{w'w'})/U_\infty^2 = (2/3)\kappa/U_\infty^2$ is set as 0.05%, as measured in wind tunnel (Crompton, 2000). Constant pressure equal to the freestream p_∞ was set at the outlet.

Figure 2. Thin flat plate dimensions.

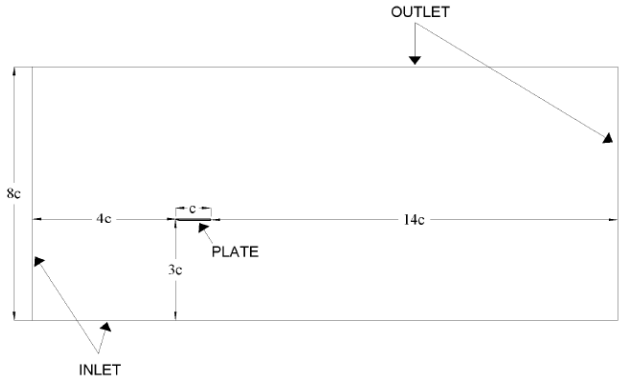

Figure 3. Domain details.

The mesh was created with 1.5×10^5 cells, a slightly larger number of points than employed by Collie (2005), based on a grid convergence study performed by him. The distance of first node above the plate was designed as 6.25×10^{-5} c (c is the length of the chord) to guarantee $y^+=(\tau_s/\rho)^{0.5}\, y/\upsilon$ around 1, which is the value indicated for both RANS, where τ_s is the wall shear stress.

To flow field was determined with the commercial software Fluent (2006) with both models described in section 2. This code is based in Finite Volume Method. Simulations were obtained with the QUICK scheme (Leonard, 1979), which is second order. The pressure-velocity coupling was handled by the SIMPLE algorithm. The system of algebraic equation was solved with the Multgrid method (Hutchinson and Raithby, 1986). The problem was considered converged when the maximum residue of all equations was smaller than 10^{-6}.

3.2. Reattachment length

Table 1 presents the reattachment lengths (X_R) for the flat plate at 1°, 2°, 3°, 4° and 5° incidence angles, obtained by turbulence models.

Table 1 – Normalized reattachment lengths (X_R) and respective errors.

	X_R/c (θ=1°)	error	X_R/c (θ=2°)	error	X_R/c (θ=3°)	error	X_R/c (θ=4°)	error	X_R/c (θ=5°)	error
Experimental (Crompton, 2000)	0.140		0.272		0.470		0.728		0.942	
SA (present work)	0.152	8.4 %	0.278	2.2 %	0.463	1.5 %	0.712	2.2 %	0.956	1.5 %
SST (present work)	0.146	3.9 %	0.292	7.4 %	0.440	6.3 %	0.735	1.0 %	0.906	3.8 %
κ–ω (Collie, 2005)	0.184	24 %	-	-	0.510	8.4 %	-	-	-	-
SST (Collie, 2005)	0.149	5.8 %	-	-	0.437	6.4 %	-	-	-	-
f-LES (Sampaio et al. 2006)	0.136	3.0 %	-	-	-	-	-	-	-	-
LES Dinamic (Rezende & Nieckele, 2009)	0.141	0.6 %	-	-	-	-	-	-	-	-

The prediction accuracy of the reattachment lengths for this flow is strongly dependent on the ability of the turbulence model to represent the complex flow structure described; however the mesh refinement also plays a crucial part on this performance. It can be seen in Table 2, that the worse prediction was obtained with κ–ω model due to its deficiency in accurately predicting the free stream flow. Although the Spalart-Allmaras model predicted a better results than the κ–ω model, Rezende & Nieckele (2009) showed that this model is not able to predict the normal turbulent fluctuations. Since the SST κ–ω model blends the precise formulation of the κ–ω model close to walls with the free-stream independence of the κ–ε model outside the boundary layer, smaller errors in the X_r values were obtained. Note

the improvement in the result reached here with the SST κ–ω model in relation to the one obtained with the same model by Collie et al. (2008), which shows the influence of a more refined mesh. Finally, For the inclination angle equal to 1°, it is evident in Table 2 that the LES Dynamic model, with more refined mesh, provided the best result, not only because it can capture the large structures, but also the transfer of energy between scales and its dissipation at the small scales. It is believed that the f-LES prediction needs a more refined mesh to produce accurate X_r result.

3.2. Mean velocities profiles

The mean velocities profiles obtained with SST and Spalart-Allmaras (SA) models for the incidence angles θ = 1° , 2°, 3°, 4° and 5° are compared with the experimental data de Crompton (2000) at three stations in Figs. 4, 5, 6, 7 and 8, respectively. All stations are located inside the bubble for θ = 3°, 4° and 5°, but for θ = 1° and 2° the third station is outside the bubble. For the θ=1° case, the LES results (Sampaio et al, 2006a) are also included in Fig. 4.

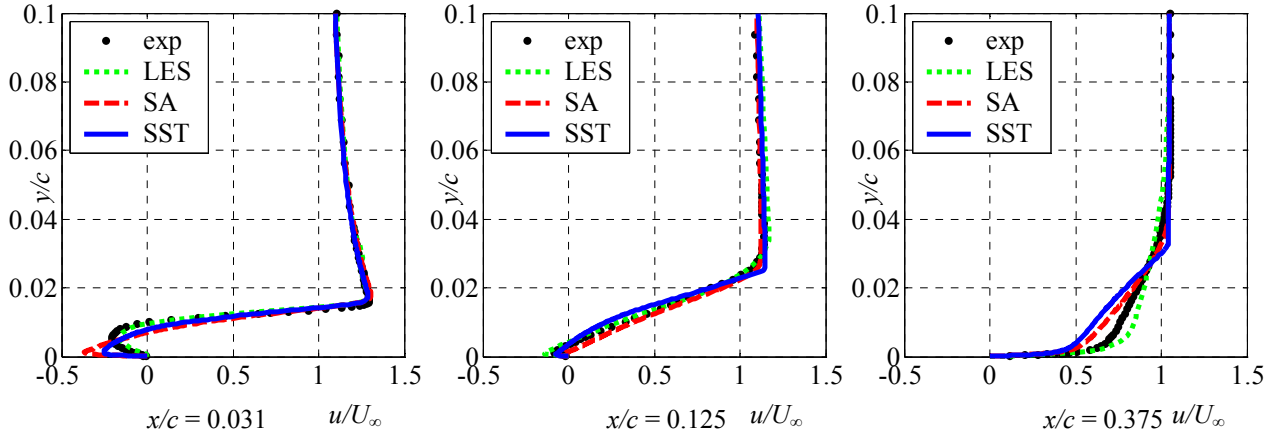

Figure 4. Velocities profiles for incidence angle θ =1° .

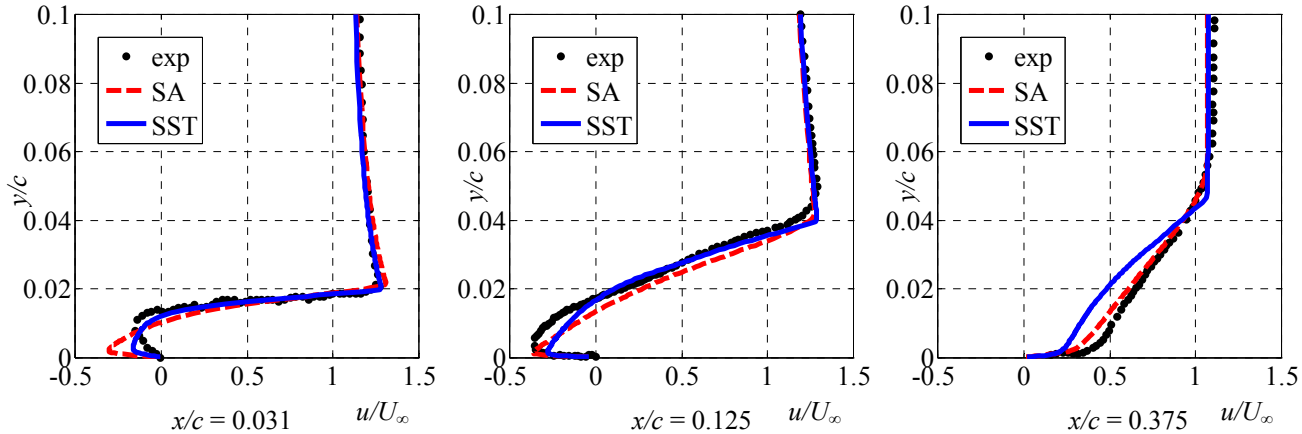

Figure 5. Velocities profiles for incidence angle θ =2° .

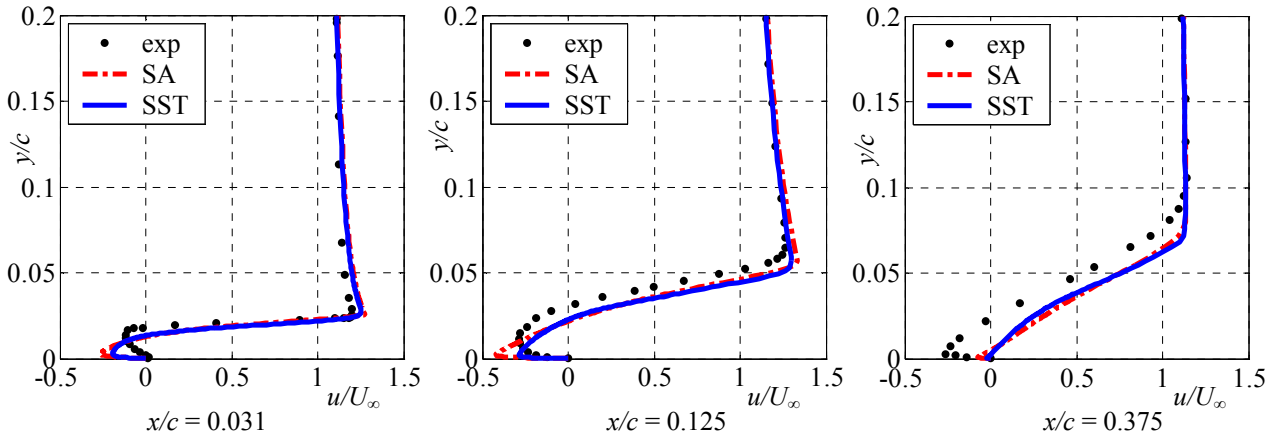

Figure 6. Velocities profiles for incidence angle θ =3°.

The reversed flow in the leading edge bubble experiences relaminarisation and the boundary layer begins to show very laminar features. The velocity profiles, in the two initial stations (x/c = 0.031 ; 0.125) of Figs. 4 and 5, and in all other stations of Figs. 6, 7 and 8, which are inside the bubble, show that the experimental data has a more laminar profile in comparison with the RANS turbulence models results which all experience a sharp increase in velocity over the near-wall region, specially the SA model. To simulate the process of relaminarization an appropriate transition model is required which is not provided by the RANS models investigated, consequently these models predict greater velocity gradient in this wall region. On the other hand, for the θ=1° case, the LES results (Sampaio et al, 2006) showed an excellent agreement with experimental data for the two first stations inside the bubble (Figs. 4a and b). However, the agreement deteriorates at station 3, outside the bubble (Fig. 4c), where the velocity recovery is slower, while the RANS models predict a faster recovery. Collie (2008) attributes this difference between the turbulence models and experimental results to the influence of wind tunnel in the boundary layer, however, this assessment is difficult to quantify. Sampaio et al (2006) attributed the discrepancy the LES model with the experimental data at this station to the mesh refinement. The present paper prefers to explain the discrepancies of the RANS models to their inability to capture the anisotropy of flow near the wall.

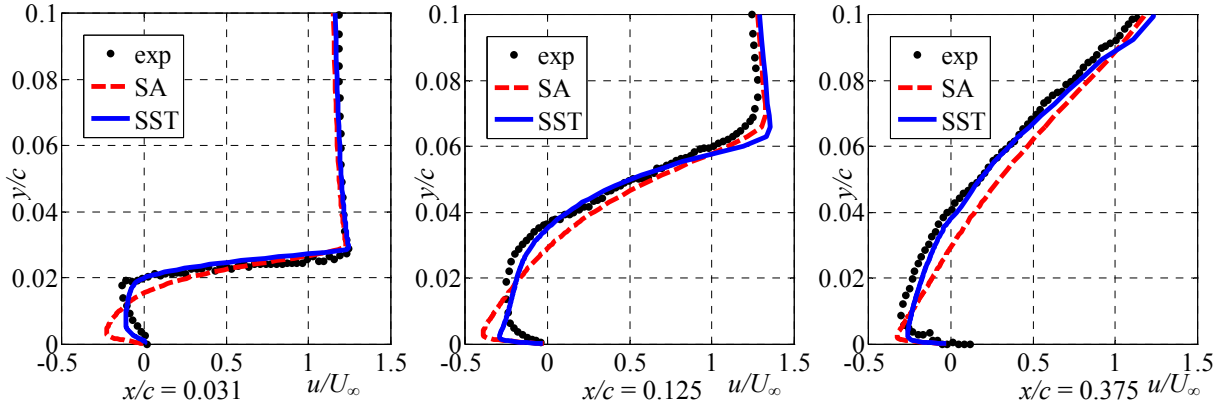

Figure 7. Velocities profiles for incidence angle θ =4° .

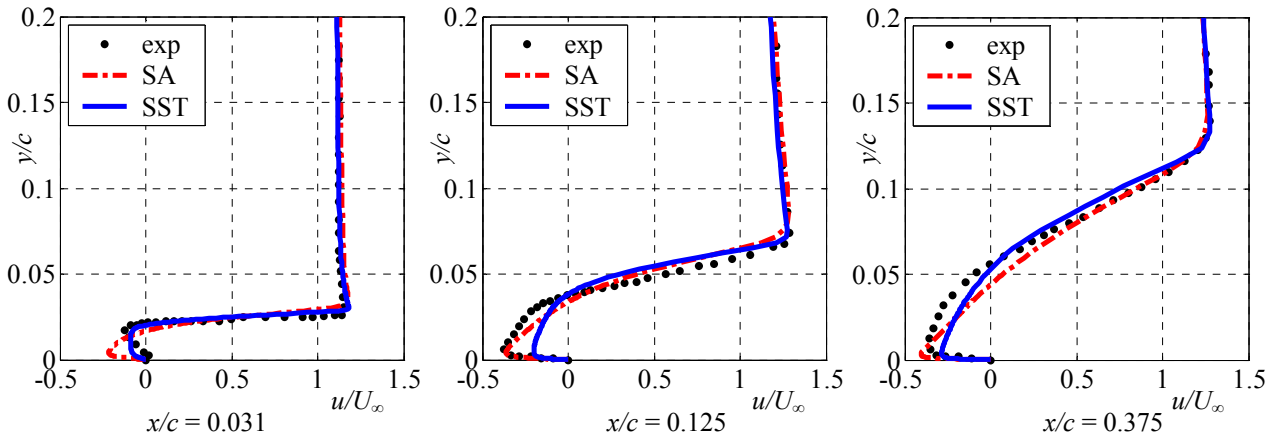

Figure 8. Velocities profiles for incidence angle θ =5° .

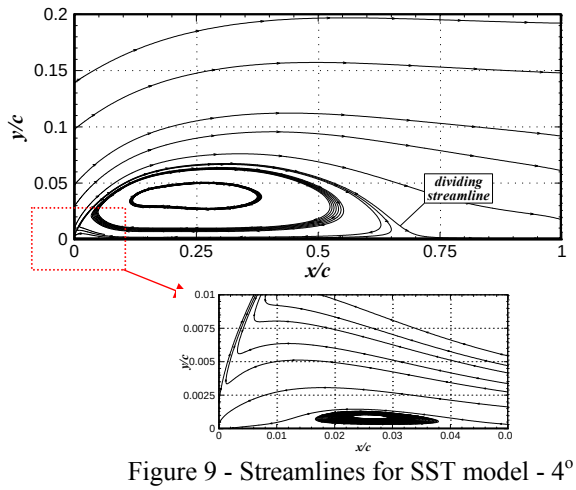

Figure 9 - Streamlines for SST model - 4°

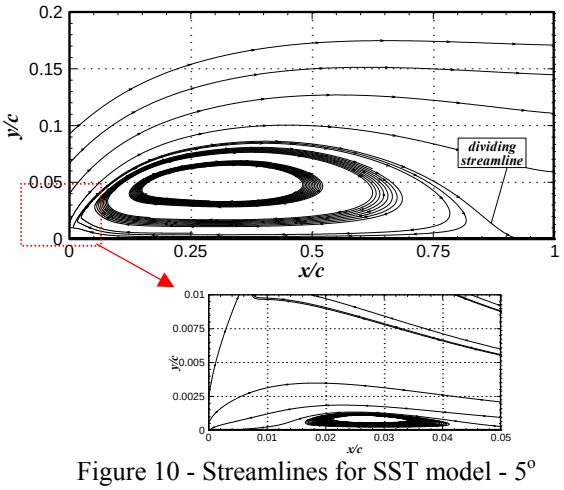

Figure 10 - Streamlines for SST model - 5°

Figures 9 and 10 shows the streamlines corresponding to the predictions of SST model. It can be verified that the SST model was able to predict the second recirculation bubble, which is observed experimentally. The Spalart-Allmaras model not presents the secondary and it is directly related to the more turbulent velocities profiles observed in the results of those simulations, inducing the flow inside the bubble to be more resistant to the second separation, keeping the reverse boundary layer attached to the plate inside the main bubble. Comparing the streamlines obtained with the SST model, it can be seen that the presence of the secondary bubble displaces the center of the main recirculating bubble downstream.

3.2. Pressure Distributions

The pressure distribution is analyzed through the pressure coefficient defined as

$$C_P = (p_\infty - p)/(0.5\ \rho\ U_\infty^2) \tag{5}$$

where p is the static pressure, p_∞ and U_∞ are the freestream pressure and velocity.

Figure 11 presents the variation of the pressure coefficient along the plate for θ =1°. Again the RANS models SA and SST are compared with the experimental data. These results confirm the discussion of the previous section, i.e., the turbulence models overpredict the velocity magnitude near the wall, therefore, as expected the pressure distribution is underpredict. In Figure 11, the LES results of Sampaio et al. (2006) were also included. It can be seen a pressure peak displaced from the leading edge as the experimental data, however the pressure peak was also underpredicted as the RANS results. Further, the pressure coefficient drop of LES is steeper and delayed, in relation to the experimental data. Both RANS models underpredicted the pressure coefficient downstream of the reattachment point, where the LES results for θ=1° was quite good.

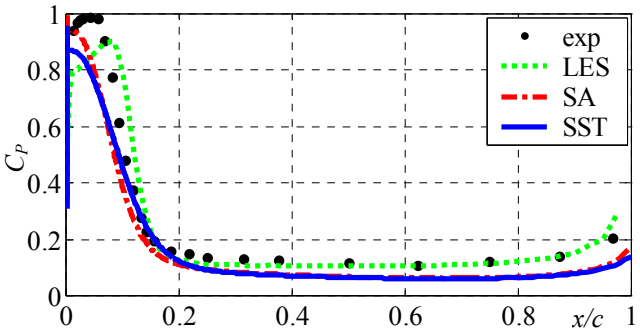

Figure 11. Pressure Coefficient for angle of attack 1°

Figures 12 and 13 presents pressure contours near the leading edge, obtained with SST model, where the stagnation point in the lower side of the plate can be clearly seen. A visible suction can also be seen inside the bubble region, in the upper side of the plate, by the significant pressure reduction.

Figure 12. Isolines of constant pressure for 2°

Figure 13. Isolines of constant pressure for 4°

In the interior of the thin airfoil bubble the pressure is mainly determined by the shear layer curvature, in other words, stronger streamline curvature will lead to smaller pressure. Due to the difficulty of the turbulence models to predict with accuracy the transition position and resolution of the secondary bubble, these models demonstrate an inferior and flatter suction peak. Larger discrepancies between the predictions and the experimental data are observed as he angle of attack increases. These discrepancies are associated with the inability of the models to predict the complex flow inside the bubble. Large angles of attack are associated with longer bubbles; therefore, worse predictions are obtained. These results encourage the investigation of these higher angles with LES, in spite of being much more expensive.

3.3. Second order statistics

The turbulent second order statistics $\overline{u'u'}$ predicted with SA and SST are compared with the experimental data in Figs. 14, 15, 16, 17 and 18 for the five angles of incidence. For θ=1°, the LES results of Sampaio et al (2006) are also included in Fig. 14, where it can be seen that at the first station the production of turbulence is underpredicted resulting in smaller $\overline{u'u'}$, being overpredicted at x/c=0.125, what is in agreement with the displaced pressure peak observed in Fig 8a. After the reattachment point, its predictions are superior to the RANS predictions.

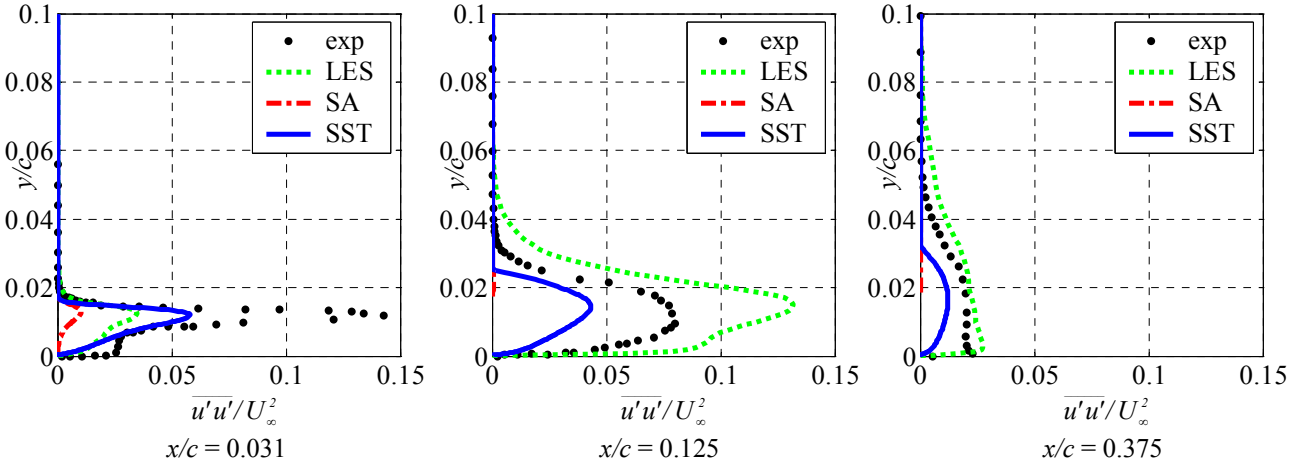

Figure 14. Second order statistics for angle of attack 1° .

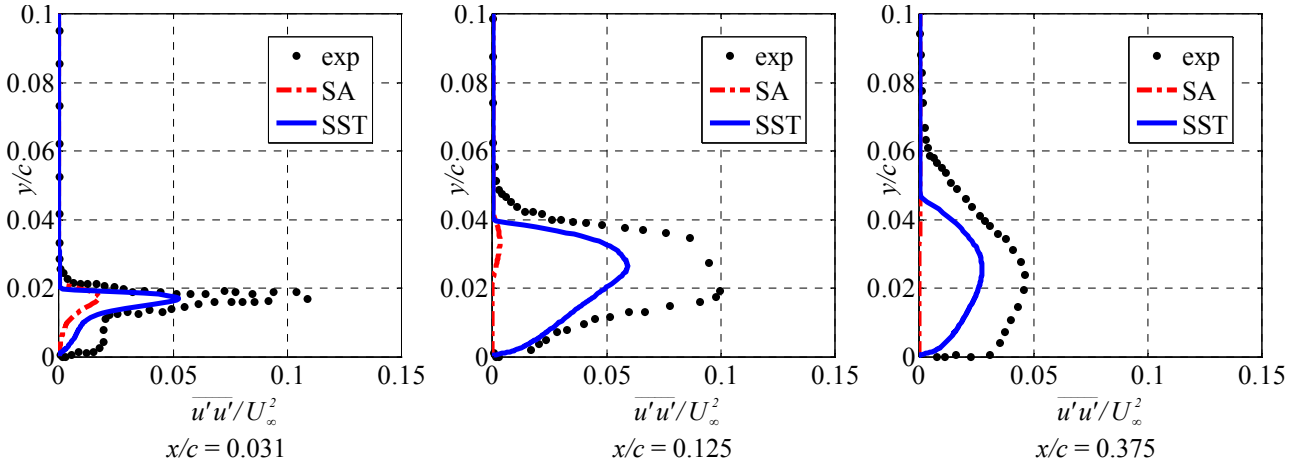

Figure 15. Second order statistics for angle of attack 2° .

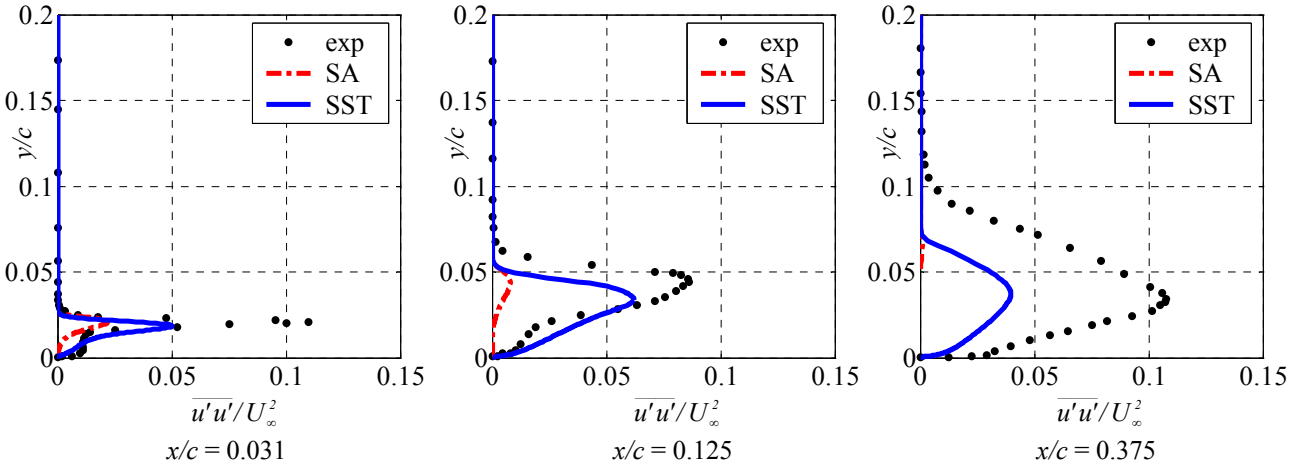

Figure 16. Second order statistics for angle of attack 3° .

The Spalart-Allmaras model uses a viscous damping function to better represent the buffer layer and viscous sublayer, but this feature results in a major damping of entrainment rate and consequently smaller turbulence levels inside the bubble, which are visible in all stations for the three cases shown in Figs. 14, 15, 16, 17 and 18.

The SST model simulates more turbulence in the shear layer than the Spalart-Allmaras model. For turbulent boundary layers the SST model uses standard κ–ω in the near-wall region and then blends to the standard κ–ε model across the outer region of boundary layer. Nevertheless inside the thin airfoil bubble the SST model blends κ–ε across the inner region of the bubble so that the ε–equation is solved across the shear layer. Therefore it appears that the ε–equation predicts a lower dissipation of turbulence which leads an over prediction of turbulence in the separated shear layer. Thus the increase of turbulence is a direct result of the ε–equation which actually improves SST results. This effect is partially compensating for the model's inability to predict the increase in the turbulence entrainment.

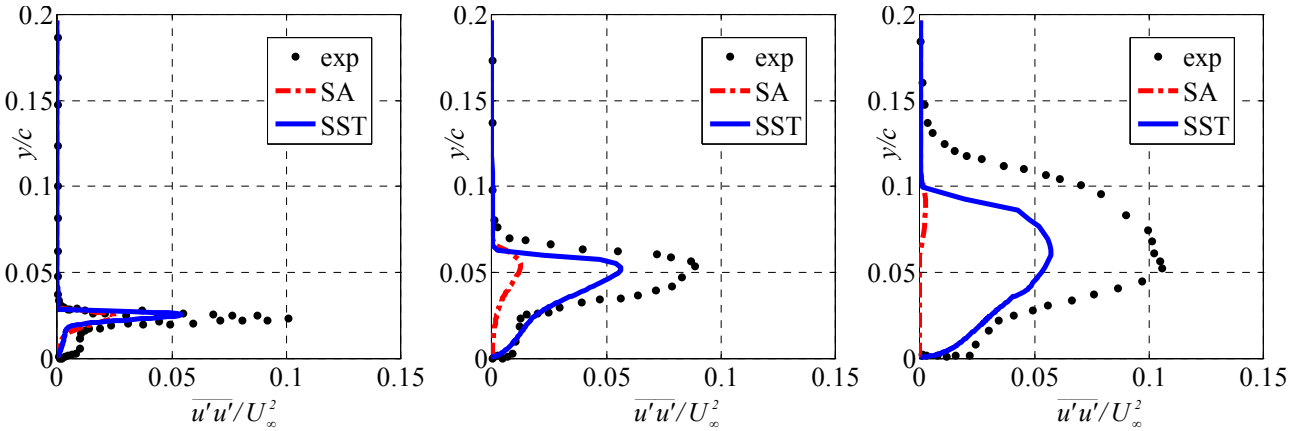

Figure 17. Second order statistics for angle of attack 4° .

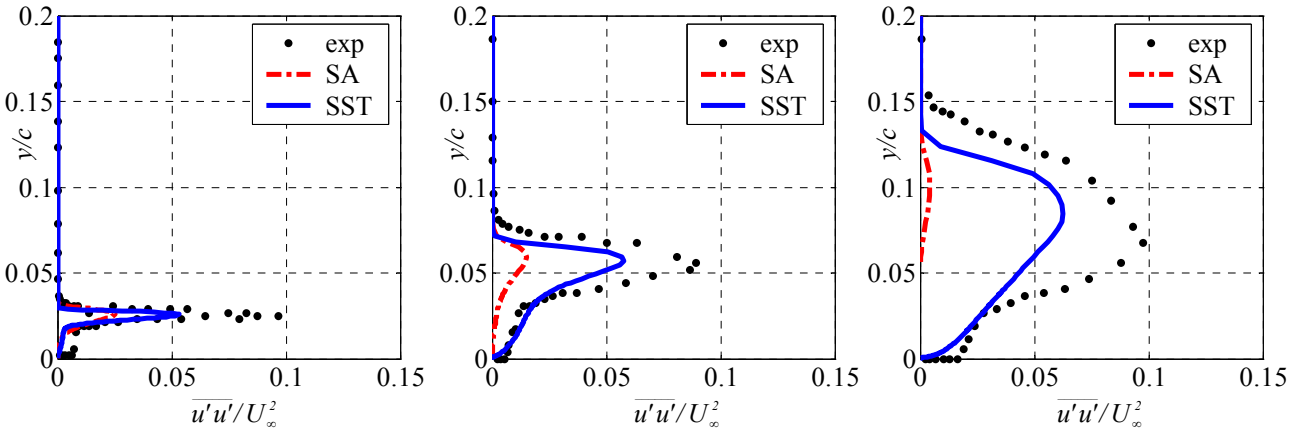

Figure 18. Second order statistics for angle of attack 5° .

4. CONCLUSION

In this work, the turbulence models of SST (Menter, 1994) and Spalart-Allmaras (1992) were applied to calculate the incompressible flow over a flat plate with a sharp leading edge, with small inclination angles. Five different angles were investigated θ=1° from 5°. The results obtained were compared with experimental data of Crompton (2000). For θ=1° the solution was also compared with available LES results (Sampaio, 2006).

The mean profiles velocities presented reasonable agreement with the experimental results; however the details of the recirculating bubble were underpredicted in size and over predicted in magnitude. Qualitatively the profiles are the same for the different angles of attach indicating the presence of similarity. The prediction of the reattachment length was improved with the increase of the angle of attack; on the other hand, the pressure distribution over the plate has deteriorated. The LES model prediction was slightly superior in relation to the pressure distribution for θ=1°, as well as the second order statistics. Although a better prediction of the reattachment length was obtained with the SA model, the overall results of the SST were better. The Spalart-Allmaras model did not capture the second recirculation bubble and a correct entrainment in the boundary shear layer, causing deviations in the velocity and pressure field in the bubble region. The SST model predicted this structure for $\theta = 4^0$ and 5^0, contradicting the conclusions of Collie et al. (2008) and

Sampaio et al. (2006).

The difficulty to capture the entrainment of the separated shear layer, encourage the investigation of the problem with more demanding models such as LES and DNS.

5. ACKNOWLEDGEMENTS

The authors acknowledge the support awarded to this research by the Brazilian Research Council, CNPq.
The authors acknowledge the support awarded to this research by the Brazilian Research Coordinate, CAPES.

6. REFERENCES

Cazalbou, J.B., Spalart, P.R., Bradshaw, P., 1993, "On the Behavior of 2-Equation Models at the Edge of a Turbulent Region", Physics of Fluids, Vol. 6, No. 5, pp. 1797-1804.

Collie S., Gerritsen M., Jackson P., 2008, "Performance of Two-Equation Turbulence Models for Flat Plate Flows with Leading Edge Bubbles". Journal of Fluids Engineering-Transactions of the Asme, Vol. 130, No. 2.

Crompton, M. J.; Barret, R. V., 2000, "Investigation of the Separation Bubble Formed Behind the Sharp Leading Edge of a Flat Plate at Incidence". Proceedings of the Institution of Mechanical Engineers Part G-Journal of Aerospace Engineering, Vol. 214, No. G3, pp. 157-176.

Durbin, P.A., 1995, "Separated Flow Computations with κ - ε - v^2 Model". AIAA Journal, Vol. 33, No. 4, pp. 659-664.

Gault, D. E., 1957, An investigation at low speed of the _ow over a simulated _at plate at small angles of attack using pitot static and hot-wire probes, Technical Report TN-3876, NACA.

Germano, M., Piomelli, U., Moin, P., Cabot, W. H., 1991, "A Dynamic Subgrid-Scale Eddy Viscosity Model". Phys. Fluids A, Vol. 3, No. 7, pp. 1760-1765.

Hutchinson, B. R., and Raithby, G.D., 1986, "A Multgrid Method Based on the Additive Correction Strategy", Numerical Heat Transfer, vol. 9, pp.511-537.

Launder B. E., 1989, "Second-Moment Closure: Present... and Future?" , International Journal of Heat and Fluid Flow, Vol. 10, No. 4, pp. 282-300.

Leonard, B.P. 1979, "A Stable Accurate Convective Modeling Procedure Based on Quadratic Upstream Interpolation", Computer Methods in Appied. Mechanics and Engineering, Vol.19, pp. 59-88.

Lilly, D. K., 1992, "A Proposed Modification of the Germano Subgrid-Scale Closure Method**"**. Physics of Fluids A, Vol. 4, No. 3, pp. 633-635.

Menter, F. R., 1994, "Two-Equation Eddy-Viscosity Turbulence Models for Engineering Applications", AIAA Jounal, Vol. 32, No. 8, pp. 1598-1605.

Newman Bg, Tse Mc, 1992, "Incompressible-Flow Past A Flat-Plate Aerofoil With Leading-Edge Separation Bubble", Aeronautical Journal Vol. 96 (952), pp. 57-64.

Rezende, A.L.T. Sampaio, L.E.B and Nieckele, A.O., 2008, "Reynolds Average Navier-Stokes Simulation of Highly Anisotropic Turbulence Structures", Proceedings of the 6th Spring School of Transition and Turbulence, EPTT 2008.

Rezende, A.L.T., Nieckele, A.O., 2009, "Evaluation Of Turbulence Models To Predict The Edge Separation Bubble Over A Thin Aerofoil", Proceedings of the 20th International Congress of Mechanical Engineering – COBEM 2009

Sampaio, L.E.B. Nieckele, A. O., Gerritsen, M. and Collie, S., 2006, "Numerical Simulations Of The Long Recirculation Bubbles Formed In Incompressible Aerodynamic Flows Over Thin Flat Plates At Shallow Incidence", Proceedings of the 11th Brazilian Congress of Thermal Sciences and Engineering -- ENCIT 2006, Paper CIT06-0278

Spalart, P., Allmaras, S., 1992, "A one-equation turbulence model for aerodynamic flows", Technical Report AIAA-92-0439, American Institute of Aeronautics and Astronautics.

Wilcox, D.C., 1998, "Turbulence Modeling for CFD". Ed. DCW, Califórnia, EUA.

7. RESPONSIBILITY NOTICE

The authors are the only responsible for the printed material included in this paper.